

MARTIN MARIETTA ENERGY SYSTEMS LIBRARIES



3 4456 0365934 2

ORNL-3457
UC-34 - Physics
TID-4500 (20th ed.)

THE DEPTH-DOSE DISTRIBUTION PRODUCED IN A
SPHERICAL WATER-FILLED PHANTOM BY THE
INTERACTIONS OF A 160-MeV PROTON BEAM

F. C. Maienschein
T. V. Blosser



OAK RIDGE NATIONAL LABORATORY

operated by

UNION CARBIDE CORPORATION

for the

U.S. ATOMIC ENERGY COMMISSION

CENTRAL RESEARCH LIBRARY

DOCUMENT COLLECTION

LIBRARY LOAN COPY

DO NOT TRANSFER TO ANOTHER PERSON

If you wish someone else to see this
document, send in name with document
and the library will arrange a loan.

Printed in USA. Price: \$0.75 Available from the
Office of Technical Services
U. S. Department of Commerce
Washington 25, D. C.

LEGAL NOTICE

This report was prepared as an account of Government sponsored work. Neither the United States, nor the Commission, nor any person acting on behalf of the Commission:

- A. Makes any warranty or representation, expressed or implied, with respect to the accuracy, completeness, or usefulness of the information contained in this report, or that the use of any information, apparatus, method, or process disclosed in this report may not infringe privately owned rights; or
- B. Assumes any liabilities with respect to the use of, or for damages resulting from the use of any information, apparatus, method, or process disclosed in this report.

As used in the above, "person acting on behalf of the Commission" includes any employee or contractor of the Commission, or employee of such contractor, to the extent that such employee or contractor of the Commission, or employee of such contractor prepares, disseminates, or provides access to, any information pursuant to his employment or contract with the Commission, or his employment with such contractor.

ERRATA -- ORNL-3457

- \ Page 12, line 3: Change sentence to read "The radial distribution of protons was approximately"
- \ Page 14, line 8: Change to read " $(1.34 \pm 0.01) \times 10^{-10}$ amps....."

ORNL-3457

Contract No. W-7405-eng-26

Neutron Physics Division

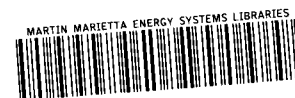
THE DEPTH-DOSE DISTRIBUTION PRODUCED IN A SPHERICAL
WATER-FILLED PHANTOM BY THE INTERACTIONS
OF A 160-MeV PROTON BEAM

F. C. Maienschein
T. V. Blosser

Date Issued

JUN 7 1963

OAK RIDGE NATIONAL LABORATORY
Oak Ridge, Tennessee
operated by
UNION CARBIDE CORPORATION
for the
U.S. ATOMIC ENERGY COMMISSION



3 4456 0365934 2



ABSTRACT

Measurements have been made of the total energy deposited at various points within a 42-cm-dia spherical water-filled lucite phantom by the secondary particles resulting from 160-MeV proton reactions with various targets. The proton source was the Harvard University Synchrocyclotron. Target materials were water, aluminum, carbon, copper and bismuth. Detectors were small lucite-walled ionization chambers filled with 97% A - 3% CO₂ or ethylene gas.

Data were taken both with the lucite phantom on the beam axis and with the phantom offset approximately 54°-43' from the beam axis. The proton beam energy determined from a part of these results, 160-162 MeV, is in good agreement with published values. The energy deposited by secondary particles was found to increase with Z, as expected. The depth-dose curves obtained have a steeply negative slope over the region near the surface of the phantom and a more gentle slope at greater depths. The magnitude of the dose in the region of the initial slope decreases with increasing target thickness. The dose in this region is presumably due to secondary protons. The magnitude of the dose at greater depths increases with increasing target thickness. At the greater depths the slope of the depth-dose curves, presumably controlled by secondary neutron interactions, is similar to that observed when the depth dose due to a Co⁶⁰ gamma-ray source was measured. A portion of the data is presented graphically and a complete tabulation of all results is included as an appendix.

TABLE OF CONTENTS

	<u>Page No.</u>
Abstract	iii
I. Introduction	1
II. Experimental Equipment	2
1. Phantom	2
2. Ion Chambers	4
3. Ion Chamber Volumes	6
4. Disposition at the Harvard Synchrotron	10
5. Current-Measuring Equipment	12
6. Beam Monitor	12
III. Measurements and Calibrations	14
1. Configurations	14
2. Calibration Factors	14
3. Backgrounds	18
IV. Discussion	20
1. Proton Beam Energy	20
2. Dose Due to Secondary Particles	22
V. Acknowledgments	25
Appendix I	28
Appendix II	30

I. INTRODUCTION

The shielding of space vehicles from the radiations in space has received considerable attention, especially since the national commitment to manned lunar and interplanetary flights.¹ At Oak Ridge National Laboratory a combination of theoretical and experimental approaches to the problem has been followed.² The primary goal of the experiments is to provide data against which the validity of calculations of proton-induced reactions in shields may be tested. Thus major emphasis in the experiments is given to the determination of secondary neutron, proton, and gamma-ray spectra. However, measurements of the ionization produced in a tissue-like material have also been made. From the ionization measurements, the energy deposited, or physical dose, was determined. These dose values, like the spectral measurements, provide a check on the calculation of secondary particle production and transport within a shield. Additionally, the dose determination in a tissue-like material requires for comparison the calculation of the penetration of secondary particles through the material, proper integration over the incident angular distributions, and appropriate flux-to-dose conversions. Over all, the complex geometry involved, together with the other requirements, provides a stringent test of the ability of the calculations to treat a realistic geometry.

Below are described dose measurements using 160-MeV protons from the Harvard University Synchrocyclotron. These measurements were originally intended only as a feasibility test of the equipment. However, the results obtained appear to contain data of useful accuracy, and no additional measurements are planned at 160 MeV. In the report an attempt has been made to assess the errors, including many arising because of the preliminary nature of the experiment which can be effectively eliminated in future work.

Succeeding portions of this report describe the experimental equipment, its disposition at the synchrocyclotron, calibration of the

-
1. Recently an entire symposium was devoted to this subject. See: Proceedings of Symposium on Protection Against Radiation Hazards in Space, Gatlinburg, Tennessee, Nov. 5-7, 1962, TID-7652 (1963).
 2. Neutron Phys. Div. Space Radiation Shielding Res. Ann. Prog. Rept. Aug. 31, 1962, ORNL-CF-62-10-29 (Rev.).

dosimeters, and the determination of the absolute proton beam intensity and energy. The results of the dose measurements are summarized and discussed. Appendices contain results of first-collision dose calculations and a complete tabulation of the experimental results.

II. EXPERIMENTAL EQUIPMENT

Differential dosimeters for use in the mixed field of secondary neutrons, protons, and gamma rays resulting from 160-MeV proton interactions with matter are not presently available, nor is the development of suitable instrumentation expected to be easy. Therefore, for the measurements discussed here a simplified approach was followed, that of determining the total energy dissipated, as measured by a small ionization chamber, at various points within a spherical water "phantom." The phantom attenuates the primary radiations and produces secondaries in a manner similar to that which occurs in tissue. The total energy deposited within the phantom may be accepted as a measure of the damage which the secondary radiations produce in tissue only in the limit that the relative biological effectiveness of all of the secondaries is equal. Measurements of absorbed energy as a function of position lead to the so-called depth dose.

1. Phantom

The phantom is a 42-cm-dia lucite sphere, shown in Fig. 1, having a wall thickness of 1.27 cm everywhere except at one point where it is diminished to 0.32 cm. When filled with water, the weight of the phantom is approximately 84 lbs. It is supported by a sturdy aluminum frame, having provision for positioning the phantom at desired angles, heights, and distances with respect to the cyclotron beam axis and target positions. The phantom can be rotated about both its horizontal and vertical axes, thus enabling depth-dose measurements throughout the sphere. With the detector inside the sphere, a control mechanism passing through a watertight ball joint allows the detector to be remotely positioned along a diameter of the sphere which intersects the thin portion of the sphere wall. Its depth is remotely read by a resistance bridge circuit to within 1 mm.

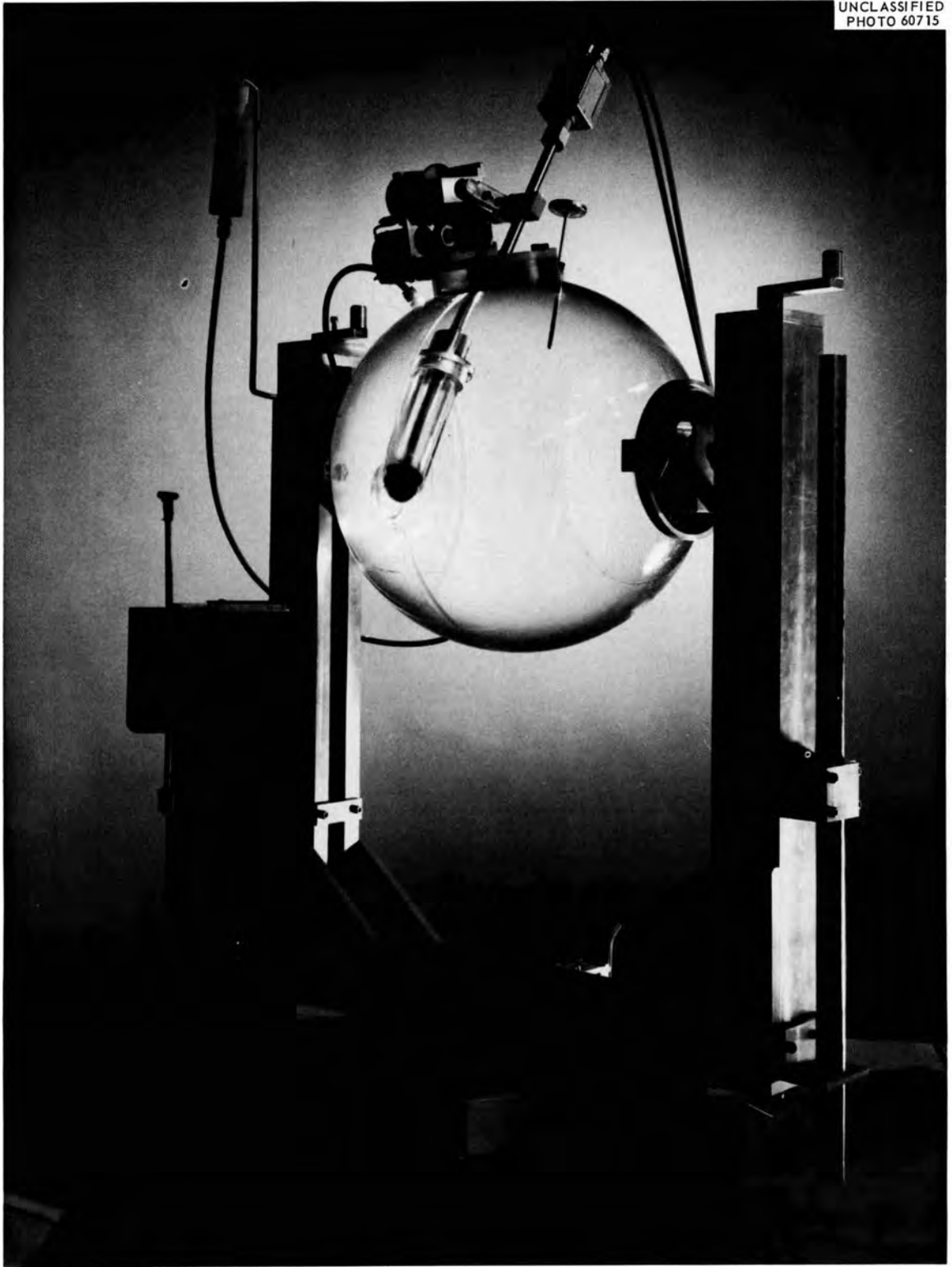


Fig. 1. The Ionization Chamber and Spherical Lucite Phantom

2. Ion Chambers

The energy deposited or absorbed at a given spot within the phantom might be measured by several means, but one of the most sensitive depends on ionization measurements in gases. Such measurements utilize the familiar Bragg-Gray relation.³ The method is based upon the concept that a small cavity, introduced in a homogeneous absorbing medium which is uniformly irradiated, is traversed by the same radiation field that exists in the medium.

The detector for the present application was designed for two situations. It must correctly measure the energy deposited at various depths in the phantom by secondaries resulting from high-energy reactions, and must respond correctly as a single-collision dose measuring instrument in air, so that calibrations against known sources may be made. A diagram of the ion chamber is shown in Fig. 2. The chamber has a 1.74-cm-radius spherical cavity, filled with either 97% A - 3% CO₂ or ethylene (C₂H₄) gas at a pressure of 1 atm. The lucite wall of the cavity is 0.32-cm thick in the forward direction. The electrical connections are made at about 10 or 12 cm from the cavity, so as to minimize the disturbance of the secondary particle equilibrium near the cavity. Lucite was chosen for the cavity wall because of its similarity in atomic composition to water. The 0.32-cm wall thickness offers little attenuation to the primary radiation, and meets the requirement of establishing secondary particle equilibrium when used with gamma-ray sources ($< \sim 1.5$ MeV) in air. The spherical cavity was chosen to simplify interpretation of the measured dose. The volume of the cavity was chosen such that when filled with the gases and at the pressure noted above, an energy deposition of $\sim 10 \text{ erg} \cdot \text{g}_{\text{H}_2\text{O}}^{-1} \cdot \text{hr}^{-1}$ produces a readily measurable current ($\sim 10^{-13}$ amp).

-
3. The Bragg-Gray relation, its application to ionization chamber dosimetry, and the conditions under which it is valid have been widely documented. See, for example, National Bureau of Standards, Handbook 75, Issued Feb. 3, 1961; also: References 4, 5, 6, and 7 below.

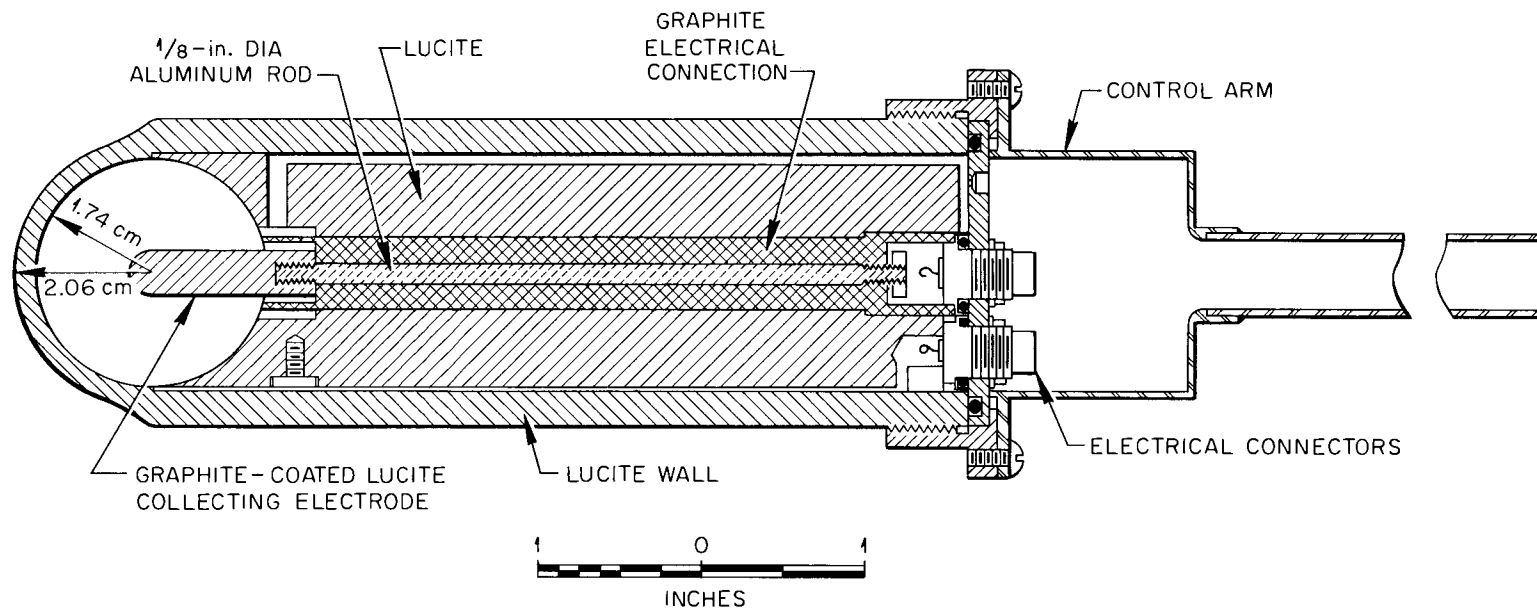


Fig. 2. Cross Section of the Ionization Chamber

Several workers^{4,5,6,7} have studied cavity ionization with respect to the error produced by variations in cavity size, wall material, and gamma-ray energy. Burch⁶ found that for a 2-cm-dia, air-equivalent wall chamber irradiated with Co⁶⁰ gamma rays the error due to electrons that do not cross the cavity is about 1%. Attix, DeLaVergne, and Ritz, experimentally,⁴ and Spencer and Attix, theoretically,⁵ have shown that the error introduced by the cavity size is small when low atomic number wall materials and gases are used.

The high voltage required to saturate the ion chamber response was determined experimentally. Current readings as a function of applied voltage are shown in Fig. 3 both for the pulsed cyclotron source and for gamma-ray and neutron sources. Only a few volts were required for saturation at the currents shown.

3. Ion Chamber Volumes

The determination of dose with an ion chamber depends upon the mass of gas contained within the chamber. With the simple spherical geometry of the chambers used in the present experiment, the volume can be calculated directly from the specified chamber dimensions and the mass computed from the volume and density. The accuracy of the value so obtained, however, may be poor because of fabrication tolerances, gas absorption or leakage, or other factors. Therefore the volume was computed from the Bragg-Gray relation on the basis of the response of the chamber to gamma rays from Co⁶⁰ and Cs¹³⁷ sources of known disintegration rates.

The Bragg-Gray relation may be written as

$$E_m = \rho_M WJ \quad (1)$$

-
4. F. H. Attix, L. DeLaVergne, and V. H. Ritz, J. Research Natl. Bur. Standards, 60, 235 (1958).
 5. L. V. Spencer and F. H. Attix, Radiation Res., 3, 239 (1955).
 6. P. R. J. Burch, Radiation Res., 3, 361 (1955).
 7. U. Fano, Radiation Res., 1, 237 (1954).

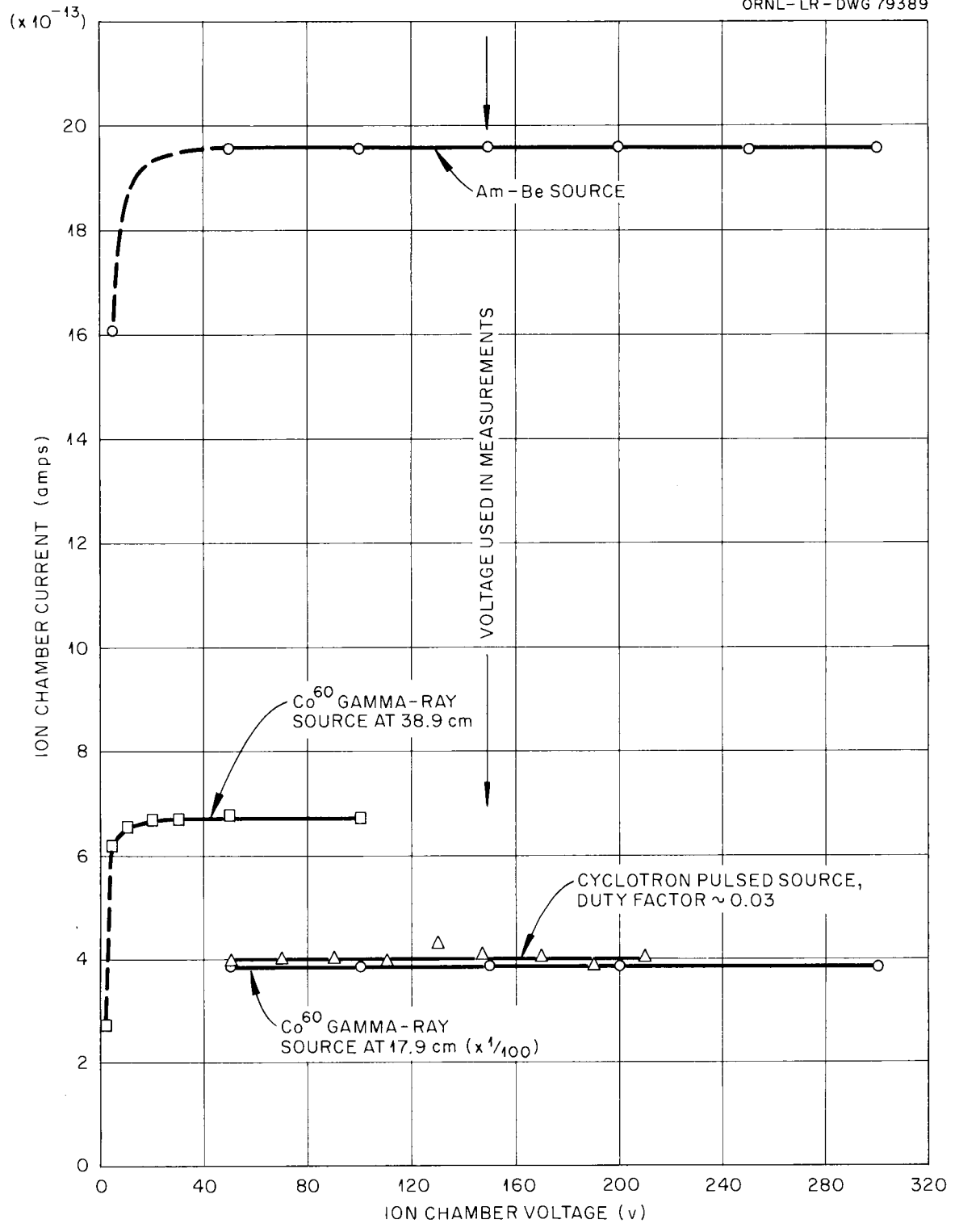


Fig. 3. Ion Chamber Response as a Function of Applied Voltage for Various Sources

where

E_m = total energy imparted to a unit mass of the chamber gas
(ev/g),

ρ_M = the ratio of the mass stopping power of the chamber wall
to that of the gas,

W = the average energy required for production of an ion pair
in the gas (ev/ip), and

J = the number of ion pairs produced per unit mass of chamber
gas (ip/g).

If $J_G = I/Vd$, where I is the current in amps measured when the chamber is exposed to a source of known disintegration rate, V is the gas volume and d its density, then Eq. 1 can be rearranged and written, with appropriate units and conversion factors as

$$V(\text{cm}^3) = \frac{I(\text{A}) \rho_M(\frac{\text{g}_G}{\text{g}_L}) W(\text{ev/ip}) 6.25 \times 10^{18} (\text{ip} \cdot \text{sec}^{-1} \cdot \text{A}^{-1}) 1.602 \times 10^{-12} (\text{erg/ev})}{d(\frac{\text{g}_G}{\text{cm}^3}) E(\text{erg} \cdot \text{g}_L^{-1} \cdot \text{sec}^{-1})} \quad (2)$$

The subscripts L and G identify lucite and gas, respectively.

For gamma radiation the energy absorbed per gram of irradiated material as a function of gamma-ray energy can be determined by calculation of the first-collision dose. Calculations were made as in NBS Handbook 75⁸ for lucite, ethylene, 97% A - 3% CO₂, water, and standard tissue. The results are tabulated and plotted in Appendix I.

The photon flux for the first-collision dose calculation was computed from the known source strengths. The Co⁶⁰ source, according to a calibration by the National Bureau of Standards produced $(2.38 \times 10^{-4}) \pm 3\%$ r/sec at 1 m. The Cs¹³⁷ source strength, determined by comparison

8. National Bureau of Standards, Handbook 75, Appendix I, Issued Feb. 3, 1961.

with a Cs¹³⁷ source calibrated in the ORNL high-pressure ion chamber, was $(3.91 \pm 0.11) \times 10^8$ photons/sec. The quantity E_m , the energy absorbed, was taken as 94.5 ergs/g_L for 1 r for the Co⁶⁰ source. For the Cs¹³⁷ source a conversion factor of 3.38×10^{-8} ergs/g_L for one photon/cm² was obtained from the first-collision dose plot. Transmission through the ion chamber wall was 0.977 for Co⁶⁰ gamma rays, 0.970 for Cs¹³⁷ gamma rays.

The stopping-power ratios for Co⁶⁰ were computed from the secondary electron spectrum produced in water⁹ and the mass stopping powers given by Nelms.¹⁰ For Cs¹³⁷ an effective average recoil energy of 260 kev was used. The stopping-power ratios are shown in the table below. The quantity W was taken as 26.0 ± 0.25 ev/ip for argon and 26.4 ± 0.22 ev/ip for ethylene.¹¹

Table 1. Stopping-Power Ratios Used in Volume Calculations

Gamma-Ray Source	ρ_M Lucite/ ρ_M Argon	ρ_M Lucite/ ρ_M Ethylene
Co ⁶⁰	1.38 ± 0.04	0.915 ± 0.02
Cs ¹³⁷	1.40 ± 0.04	0.918 ± 0.02

Current measurements were made at several source-chamber separations, using the vibrating-reed electrometer discussed later in this report. The error in J_G was estimated as $\pm 4.5\%$. From the computed values of V a weighted average was obtained, with the weighting based on the estimated errors in the source-to-chamber distance measurements, the estimated error in the electrometer scale used, and the magnitude of the background. The distance dependence was $1/r^2$ within the associated errors.

The results of the volume determinations are shown in Table 2. The calibrated volumes are in every case considerably less than that computed

9. G. J. Hine and G. L. Brownell (eds.), Radiation Dosimetry, Academic Press, New York (1956), p 25.
10. A. T. Nelms, Energy Loss and Range of Electrons and Positrons, NBS-C-577 (1956).
11. Weighted averages of values taken from the bibliography of I. T. Meyers, The Measurement of the Electron Energy Required to Produce an Ion Pair in Various Gases, HW-SA-2146 (1958). Weights were assigned whenever the authors gave no errors.

from the nominal chamber dimensions. The differences may stem from errors in pressure or temperature during filling of the chambers with the gas, or may be due to fabrication errors.

Table 2. Ion Chamber Volumes from Calibration
with Gamma-Ray Sources

Calibration Source	Argon-Filled Chamber (cm ³)	Ethylene-Filled Chamber (cm ³)
Co ⁶⁰	17.1 ± 1.2	16.3 ± 1.1
Cs ¹³⁷	16.5 ± 1.2	15.3 ± 1.2

4. Disposition at the Harvard Synchrocyclotron

The general arrangement of the experiment at the synchrocyclotron is shown in Fig. 4. The Harvard University 95-in. Synchrocyclotron is a frequency-modulated machine producing unpolarized protons at a nominal energy of 160 MeV, with an energy spread of about 2 MeV and fluxes as high as 5×10^{10} protons/sec. Its frequency range is from 23 to 30 Mc/sec, modulated by a rotating condenser. The nominal beam area is 7 cm² or less and the permanent shield consists of from 3 to 8 ft of ordinary concrete.

The proton beam emerging from the machine first passes through a vertical slit, then is deflected by the steering magnet and focused by the quadrupole magnets. The focused beam continues through a beam tube and impinges on the target. The lead bricks shown were added to reduce backgrounds during the present experiments.

A target holder is centered on the beam by adjustment of alignment posts at either end of the holder. Polaroid film, in holders that attach to the tops of the alignment posts, is used as the beam-finding sensor. The target holder is then positioned by using an alignment bar extending between the posts. For a portion of the measurements the phantom was located at 45° horizontally and vertically (below) from the beam axis. For the remainder of the measurements the phantom was located on the extension of the beam-axis, and the beam struck the phantom

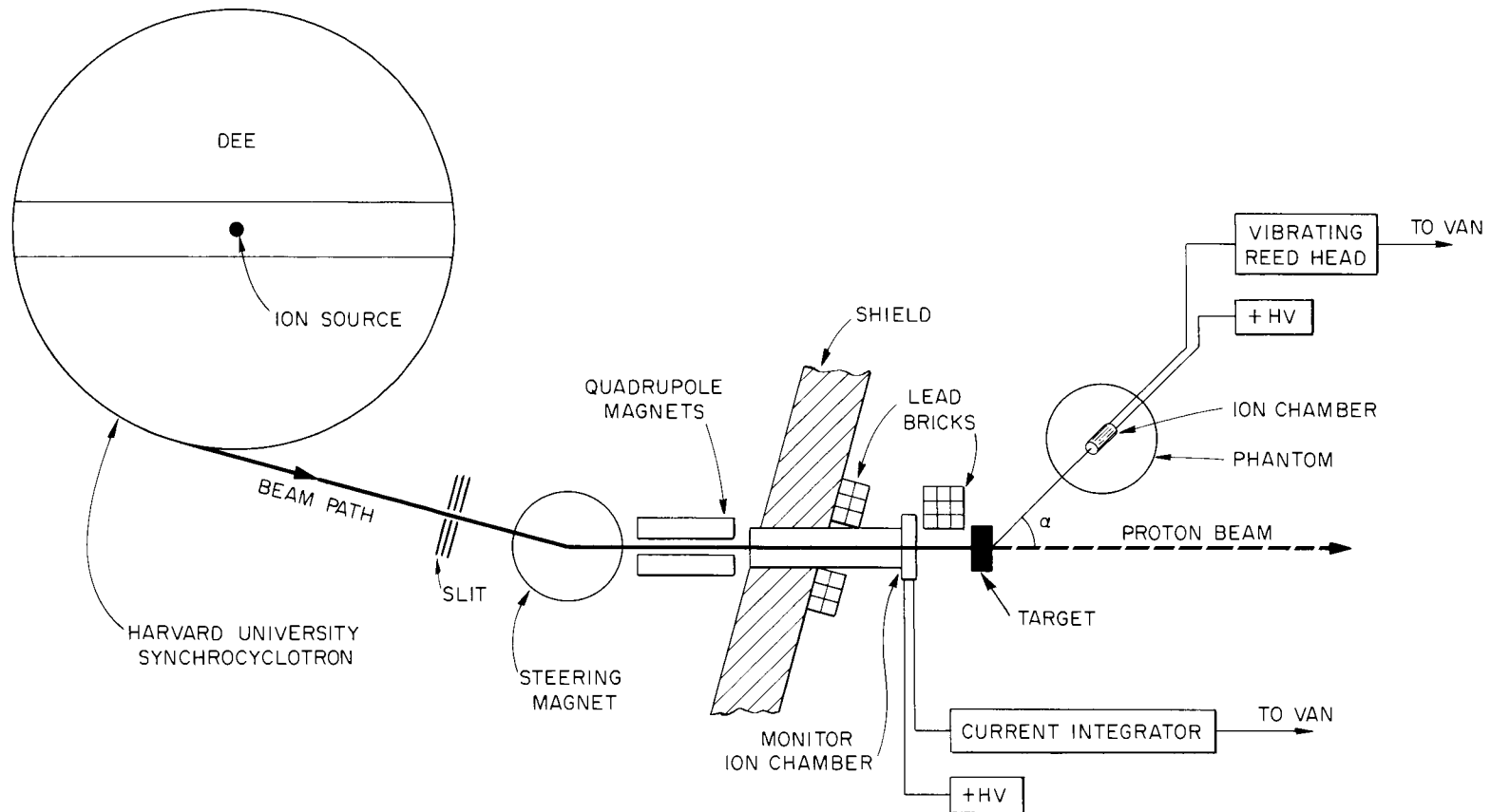


Fig. 4. General Arrangement of the Experiment at the Harvard Synchrocyclotron

directly. The beam cross section at the point of entry into the phantom was roughly elliptical, with a major axis of 2.5 cm and a minor axis of 1.6 cm. The radial distribution of protons was approximately gaussian, as determined by densitometric measurements of Polaroid negatives and by examination with a profile telescope consisting of a pair of small scintillation counters.

The electronics for the ion chamber in the phantom and the scaler for the beam monitor were remotely located in a van, and connected to the cyclotron area with 150- to 200-ft cables.

5. Current-Measuring Equipment

A block diagram of the instrumentation is shown in Fig. 5. The system is divided into two parts: a dose-determining channel and a beam-monitoring channel. In the dose-determining channel, the current produced in the ion chamber within the phantom is measured by a vibrating-reed electrometer. The electrometer can be operated either by measuring the rate of change of voltage across the vibrating capacitor or by measuring the potential difference across a high-value input resistor. The latter method was invariably used. Although the amplified current can be read from a milliammeter, an accurate meter reading is difficult to obtain because of the current fluctuations caused by variations in beam strength and other causes. Instead, the electrometer output was fed to an external recording system, a Royson Lectrocount. This system electrically integrates the fluctuating signal and transforms it to a count rate, proportional to the average current, which is recorded by a scaler unit.

6. Beam Monitor

A beam monitoring system was required in order to normalize data necessarily taken over a wide range of beam intensities. The system is based upon a specially constructed ion chamber,¹² through which the proton beam from the accelerator passes, with little absorption, enroute to the target or phantom. The current developed in the ion chamber is fed to a

12. R. T. Santoro, Measurement of the Intensity of the Proton Beam of the Harvard University Synchrocyclotron (tentative title) (to be published).

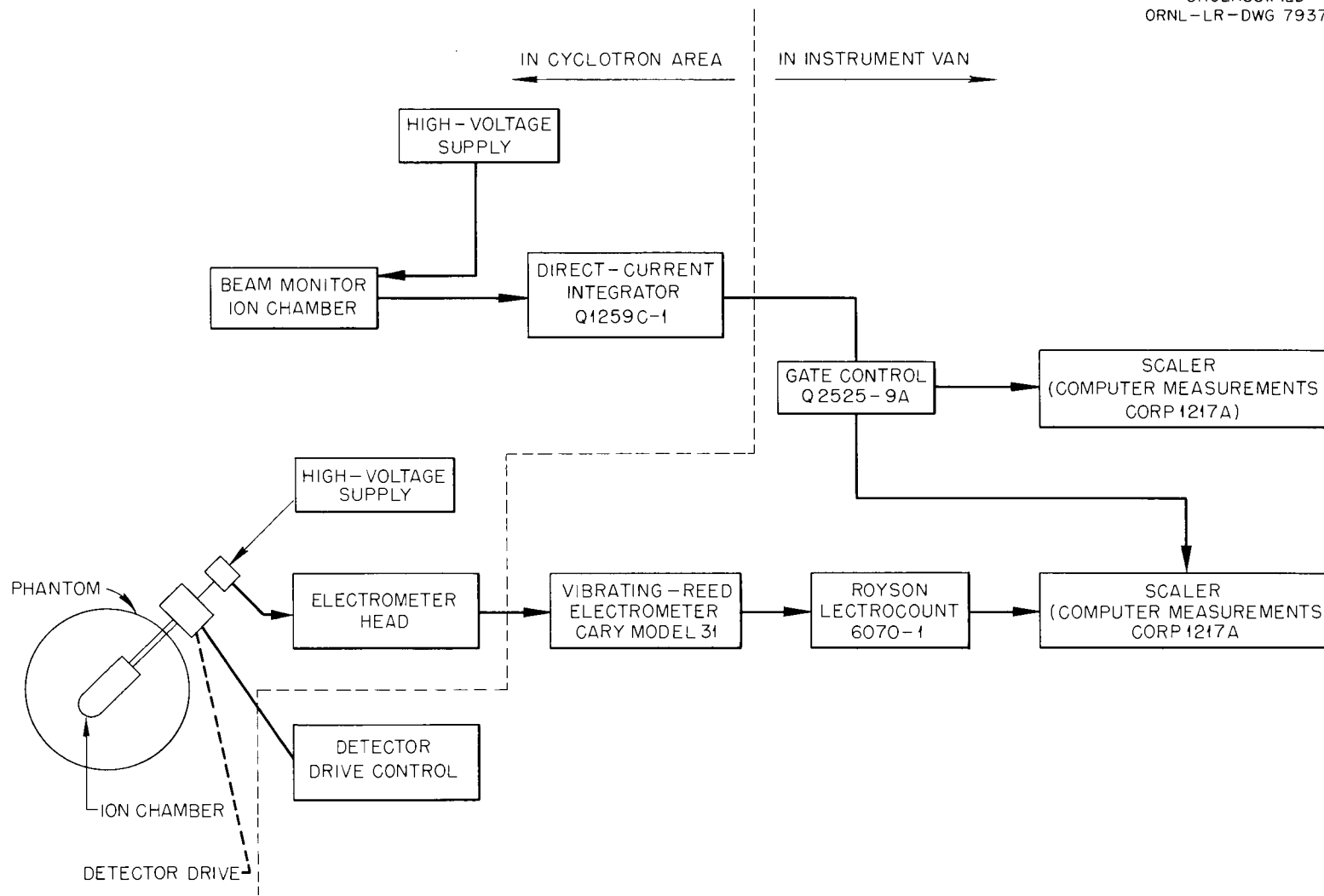


Fig. 5. Block Diagram of Instrumentation for Depth Dose Measurements

current integrator which translates the current into counts. The counts are used to control a gate circuit for the dosimeter scaler and are also recorded by another scaler.

The calibration of the specially constructed monitor ion chamber is described in detail elsewhere.¹² Briefly, the monitor ion chamber was calibrated against a Faraday cup. The current produced by the cup was determined with reference to a NBS-calibrated standard current source of $(1.34 \pm 0.01) \times 10^{10}$ amps which was loaned by A. M. Koehler of Harvard. The calibration was $(1.788 \pm 0.054) \times 10^7$ protons per monitor integrator pulse for all beam strengths used.

III. MEASUREMENTS AND CALIBRATIONS

1. Configurations

Two distinct types of measurements were made. In the primary set of measurements, targets of water, aluminum, copper, carbon, and bismuth were placed in the primary beam, and the phantom was either on the beam axis or offset at given distances and angles. Thus the energy deposited in the water phantom by the secondary particles resulting from the beam-target interactions was measured. In a subordinate series of measurements, the direct beam of protons was allowed to strike the phantom directly. In such measurements the dominant effect was produced by the primary photon beam for water thicknesses less than the proton range. Figure 6 shows the experimental geometry and defines the quantities referred to in the summary of Table 3 and in the complete tabulation of data of Appendix II.

2. Calibration Factors

The measured ionization values were converted to energy absorbed or dose by using Eq. 1. The quantities ρ_M and W of Eq. 1 are somewhat dependent upon particle type and energy, and differ from gas to gas. Values of both for argon and ethylene are shown in Tables 4 and 5. Ethylene was selected as a counter gas to minimize the variation in ρ_M , while argon demonstrates the least dependence of W on particle type and energy of any of the common gases.

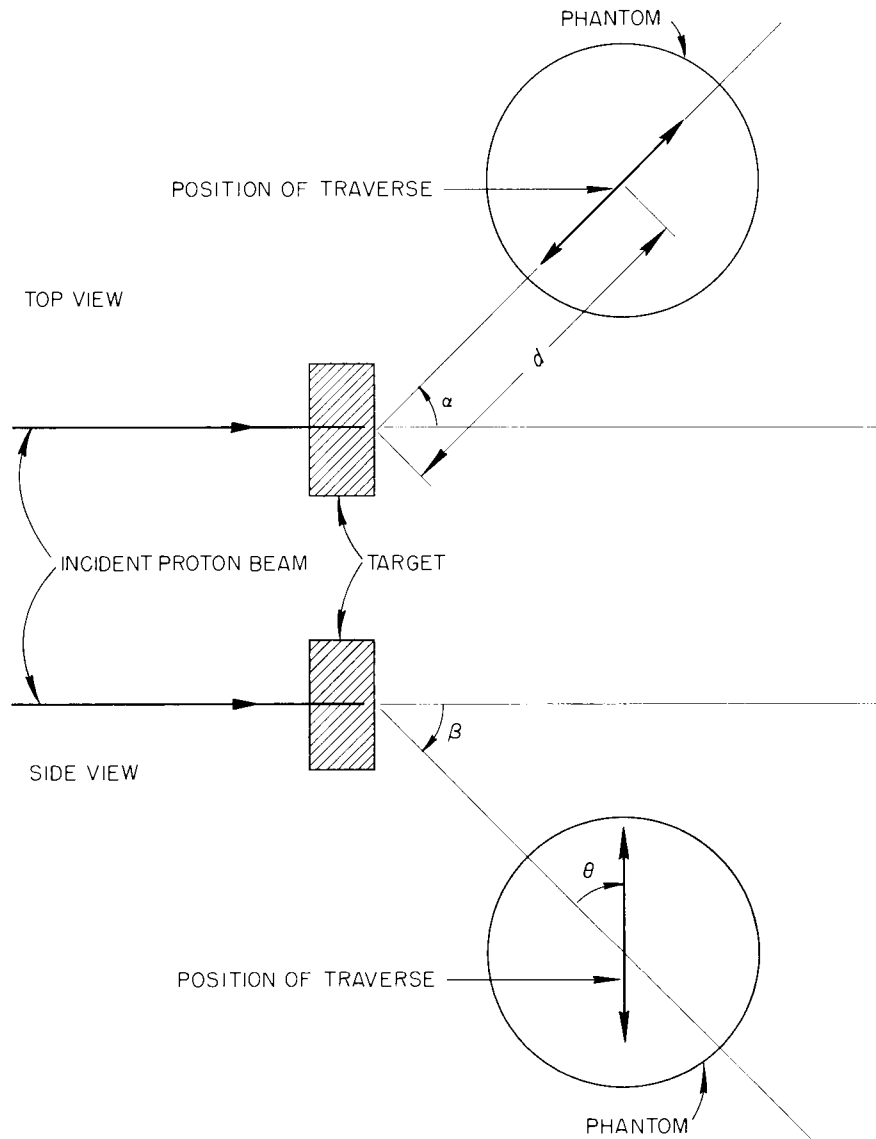
UNCLASSIFIED
ORNL-LR-DWG 79380

Fig. 6. Experimental Geometry

Table 3. Key to Experimental Configurations Studied and Locations in Which Results are Given

Target Thickness		Phantom Position Angles*		Dosimeter Traverse Angle*	Ion Chamber Type	Results	
g/cm ²	Mev	α (deg)	β (deg)	θ (deg)	Type	Fig. No.	Table No.
<u>No Target; Proton Beam Directly Incident on Phantom</u>							
		0	0	0	Both	7,8	II.1
		0	0	90	Argon		II.1
<u>No Target; Calibrated Co⁶⁰ Source</u>							
		0	0	0	Both	9	II.2
<u>Aluminum Target; Target-Phantom Distance: 48.5 cm</u>							
6.72	160-132	0	0	0	Argon	8	II.4
13.4	160-95	0	0	0	Argon	8	II.4
26.9	178	0	0	0	Both	8	II.5, II.4
26.9	178	0	0	90	Argon	11	II.5
47.0	247	0	0	0	Ethylene	8	II.4
<u>H₂O Target; Target-Phantom Distance: 48.5 cm</u>							
21.1	179	0	0	0	Argon		II.3
<u>Aluminum Target; Target-Phantom Distance: 53.7 cm</u>							
6.72	160-132	45	45	0	Argon	9	II.6
13.4	160-95	45	45	0	Argon	9	II.6
26.9	178	45	45	0	Argon	9,10	II.7
26.9	178	45	45	45	Argon	11	II.7
26.9	178	45	45	90	Argon	11	II.7
<u>Carbon Target; Target-Phantom Distance: 53.7 cm</u>							
23.3	178	45	45	0	Argon	10	II.8
<u>Copper Target; **Target-Phantom Distance: 53.7 cm</u>							
31.8	177	45	45	0	Argon	10	II.8
<u>Bismuth Target; Target-Phantom Distance: 53.7 cm</u>							
44.3	179	45	45	0	Argon	10	II.8

*See Fig. 6 for diagram defining these angles.

**20-cm-dia and 40-cm-dia copper targets; all others 20-cm-dia.

Table 4. Comparison of Stopping-Power Ratios

	Stopping-Power Ratios, ρ_M			
	<u>Lucite</u> <u>Argon</u>	<u>Water</u> <u>Argon</u>	<u>Lucite</u> <u>Ethylene</u>	<u>Water</u> <u>Ethylene</u>
Co ⁶⁰ recoil electrons	1.38	1.41	0.915	0.936
20-MeV protons	1.43*	1.46	0.914	0.928
100-MeV protons		1.49*		0.937
Average**		1.45 ± 0.04		0.934 + 0.003 - 0.006
Average,** all values:		1.43 ± 0.06		0.926 ± 0.011

*Based on data in UCRL-1325; all other values based on UCRL-2301.

**The limits are shown to indicate the spread in values.

Table 5. Average Energy, W, Required for Production of an Ion Pair*

Particle	W (ev/ip)	
	Argon	Ethylene
Gamma-ray recoil electron	26.0 ± 0.25	26.4 ± 0.22
Proton	26.4 ± 0.16	
Polonium and plutonium alpha particles	26.4 ± 0.20	28.0**
Average	26.3 ± 0.3	27.2 ± 0.8

*Weighted average of values from bibliography of Meyers (ref. 11). Weights were assigned whenever authors gave no errors. The resulting errors are probably too small.

**No error estimate given.

For gamma rays and low-energy (< 20 MeV) protons, the recoils which lead to ionization in the chamber occur largely in the lucite ion chamber wall. For neutrons and high-energy protons the pertinent recoils arise primarily in the water of the phantom. Clearly, for mixed radiations and

for a wide range of energies, significant contributions come from both regions. However, the variation in stopping-power ratios from lucite to water is seen in Table 4 to be only about 3%. For argon, the overall variation in ρ_M is $\sim 8\%$ and for ethylene only 2.5%. The values adopted for ρ_M in the data analyses, based on an average of all of the values shown in Table 4, were: for argon, 1.43 ± 0.06 ; for ethylene, 0.926 ± 0.011 . For W, on the other hand, the argon values vary only $\sim 1.5\%$, while the ethylene values for electrons and alpha particles vary 6%, with no results available for protons. The overall uncertainty resulting from the unknown character of the secondaries producing the observed ionization is about 4%.

It was unfortunately necessary to delay the absolute calibration of the ion chambers against the calibrated Co^{60} and Cs^{137} sources until several weeks after the measurements at the cyclotron were completed. Relative calibrations against an Am-Be neutron (and gamma-ray) source over this interval showed a reduction in the response of the argon chamber by a factor of 1.06 ± 0.03 and in the response of the ethylene chamber by a factor of 1.14 ± 0.07 . A possible reason for the reduction may be diffusion of gas through the counter walls, but this hypothesis has not been tested experimentally. Corrections for the lowered responses have been applied to the dose results.

After application of corrections for all effects other than particle scattering from the concrete floor of the cyclotron, the conversion factors appropriate to Eq. 1 are: The absorbed energy ($\text{erg} \cdot \text{g}_{\text{H}_2\text{O}}^{-1} \cdot \text{sec}^{-1}$) is equal to the measured ionization (amps) times $(1.40 \pm 0.14) \times 10^{10}$ for the argon-filled ion chamber and $(1.58 \pm 0.19) \times 10^{10}$ for the ethylene-filled ion chamber. The relative errors for the dose data given below are less than the absolute error, being of the order of 6%. These errors, about $\pm 10\%$ absolute and $\pm 6\%$ relative, may be applied to the results given in Appendix II.

3. Backgrounds

The background with the beam off or with the target removed was measured and shown to be small in general. The background due to particles (especially neutrons) scattered from the surroundings could not be

determined experimentally in a straightforward manner. The most important scatterer, the concrete floor, was 147 cm from the target center, while the phantom-target distance was 50 to 70 cm. If the estimate of Cook and Strayhorn¹³ for fast-neutron scattering from a concrete floor is used, the background due to floor scattering of the neutron component of the secondaries is $\sim 8\%$ for the situation in which the phantom is offset 45° horizontally and vertically (below) from the target-beam axis. The effect was, of course, decreased when the phantom was raised to the target-beam axis, being only about 3% . The effective albedo for secondary protons should be negligible and the primary beam was stopped more than 20 ft from the target. Finally, the albedo for gamma-ray scattering from the floor is of the order of one-third of that for neutrons.¹⁴

Alsmiller's calculation¹⁵ of the proportions of the three secondary components indicates that the secondary neutrons are probably dominant for the targets used. Corrections of the amounts given for neutron scattering were therefore subtracted from the otherwise corrected dose measurements. The errors were assumed as one-half of the scattering corrections, i.e., 4% and 1.5% . No scattering correction was made to the measurements without a target.

The background due to the radiation sensitivity of the electrometer reed head was made negligibly small in comparison with foreground by shielding the head with lead bricks.

A possible source of error, that due to the return by backscatter of protons into the monitor ion chamber, was found to be unmeasurable ($< 2\%$) for the target with the largest physical dimensions.

13. C. F. Cook and T. R. Strayhorn, Fast Neutron Physics, Vol. IV, Part 1 (J. B. Marion and J. L. Fowler, eds.) Interscience, New York (1960), p 812.

14. Reactor Handbook, Vol. 1, Interscience, New York (1955), p 698.

15. R. G. Alsmiller, Jr., and J. E. Murphy, Space Vehicle Shielding Studies: Calculations of the Attenuation of a Model Solar Flare and Monoenergetic Proton Beams by Aluminum Shields, ORNL-3317 (Jan. 1963); also: Neutron Phys. Div. Ann. Prog. Rept. Sept. 1, 1962, ORNL-3360, p 224; also: Ref. 2, p 145.

IV. DISCUSSION

1. Proton Beam Energy

From the results of the measurements in which the proton beam was directly incident upon the phantom, it is possible to obtain the proton range in water and thus the energy of the proton beam. The spherical shell geometry is not well suited for a range determination, but the "far" side of the Bragg peak observed is quite steep, as seen in Fig. 7. It must be noted that the depth given in the plots is measured to the center of the ion chamber. This is appropriate for the consideration of secondary particles, but for the case of the collimated proton beam the "front edge" of the chamber should be used to determine the range. The difference between the front edge and the center is 1.74 cm, the ion chamber inside radius. Measured from the front edge, the range which corresponds to a linear extrapolation to zero current in Fig. 7 is 17.9 g/cm² of water, allowing 0.6 g/cm² of water for the 1/8-in.-thick lucite shells of the phantom and the ion chamber. The energy corresponding to this range, taken from the curves of Rich and Madey,¹⁶ is 162 MeV.

The position of the peak in Fig. 7 should correspond to the mean range as measured to the average, rather than the extreme, front edge of the ion chamber. The average front edge of the chamber is 1.37 cm from its center. The range based on the peak position is 17.4 g/cm², which corresponds to a proton energy of 160 MeV (Ref. 16).

The energy values derived above are in good agreement with energy estimates based on the proton range in copper reported by Johnson¹⁷ of 160.5 ± 0.6 MeV, and are consistent with values reported earlier of 159 MeV (Ref. 18) and 158 MeV (Ref. 19).

-
16. M. Rich and R. Madey, Range-Energy Tables, UCRL-2301 (Mar., 1954).
 17. C. F. Johnson, private communication, Jan., 1963.
 18. G. Calame *et al.*, Nuclear Instruments 1, 169 (1957).
 19. F. T. Howard, Cyclotrons and High-Energy Accelerators - 1958, ORNL-2644 (Nov. 17, 1958).

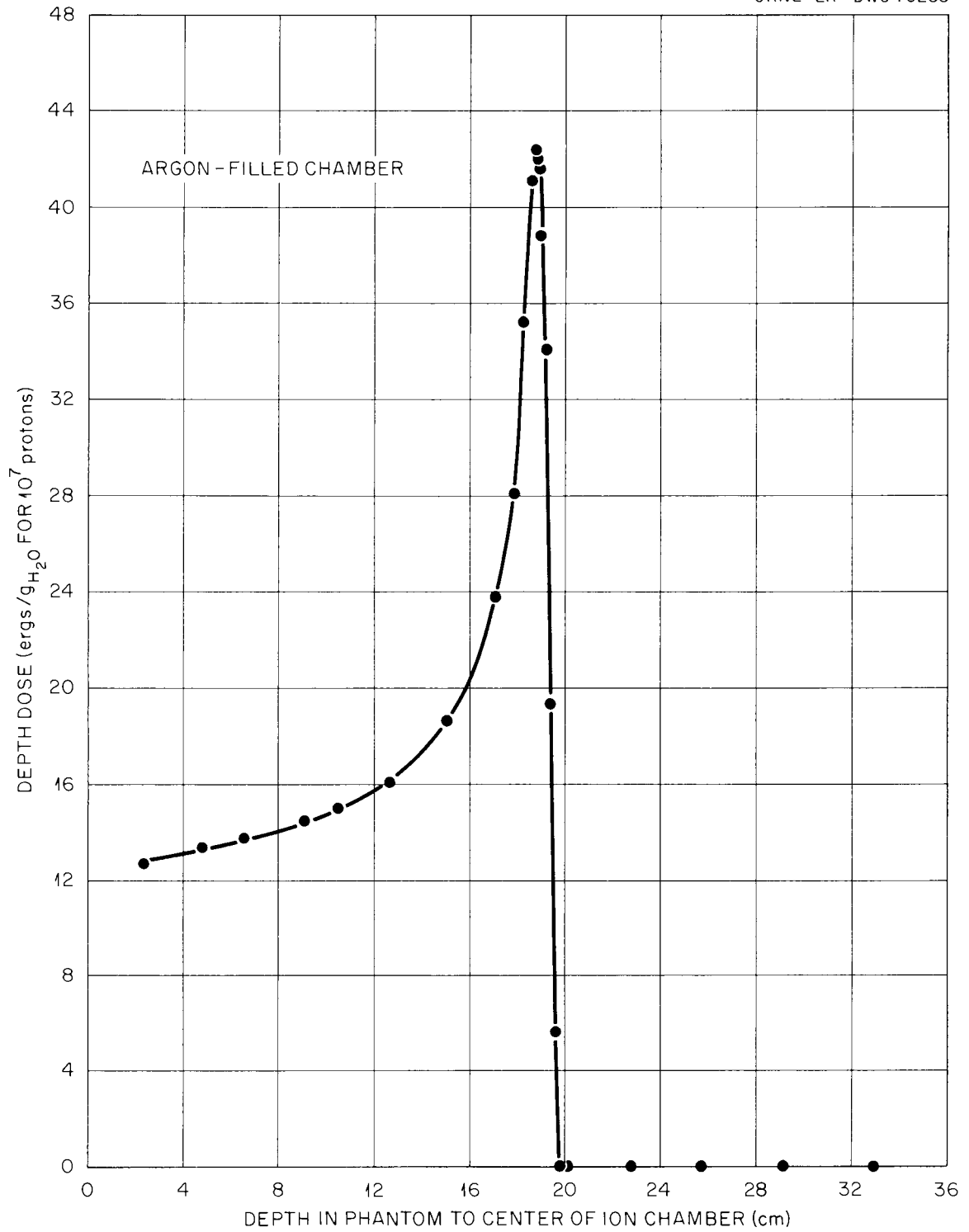


Fig. 7. Dose Deposited in Water by 10⁷ Protons Directly Incident on Phantom, as a Function of Depth

2. Dose Due to Secondary Particles

Figure 8 shows the absorbed dose as a function of depth in the phantom for aluminum targets of four thicknesses and for no target. As the figure shows, the proton beam struck the phantom both without a target and for the two thinnest aluminum targets. The depth in the phantom was measured along a diameter parallel to the proton beam axis.

The no-target results are consistent for both the ethylene-filled and 97% A - 3% CO₂-filled ion chambers. The errors for the region beyond the Bragg peak are uncertain, but large.

Since the ion chamber cross section is larger than the cross section of the proton beam, the absolute values of the absorbed dose for the thin target results should be regarded with considerable caution. Undeniable, however, is the large decrease in dose beyond the Bragg peak. Before conclusions regarding the relative importance of secondaries are drawn from Fig. 8, it should be noted that the effective solid angle is much less for the secondary particles than for the primary beam. This is particularly true for the thicker targets, within which all of the primary particles are stopped. The errors shown on some data points are intended to be representative.

The absorbed dose as a function of depth in the phantom is shown in Fig. 9 for aluminum targets of three thicknesses. The diagram shows the position of the phantom relative to the target and primary beam. No primary protons can reach the phantom in this geometry. The initially high values of dose for the 6.72 g/cm² and 13.4 g/cm² targets (both thinner than the proton range) are probably due to secondary or scattered protons. The dose due to secondaries at greater depths appears to be greater for larger target thicknesses, as might be expected. The slopes at larger distances are probably consistent within the experimental error. The lowest curve of Fig. 9 represents the depth dose resulting from the calibrated Co⁶⁰ source previously described, located, as shown in the diagram, 17.9 cm from the surface of the phantom. The slope of the dose curve due to the ~ 1.25-MeV average energy Co⁶⁰ gamma rays is quite similar to that for the secondaries from the 160-MeV protons. The secondaries from

UNCLASSIFIED
ORNL-LR-DWG 77652

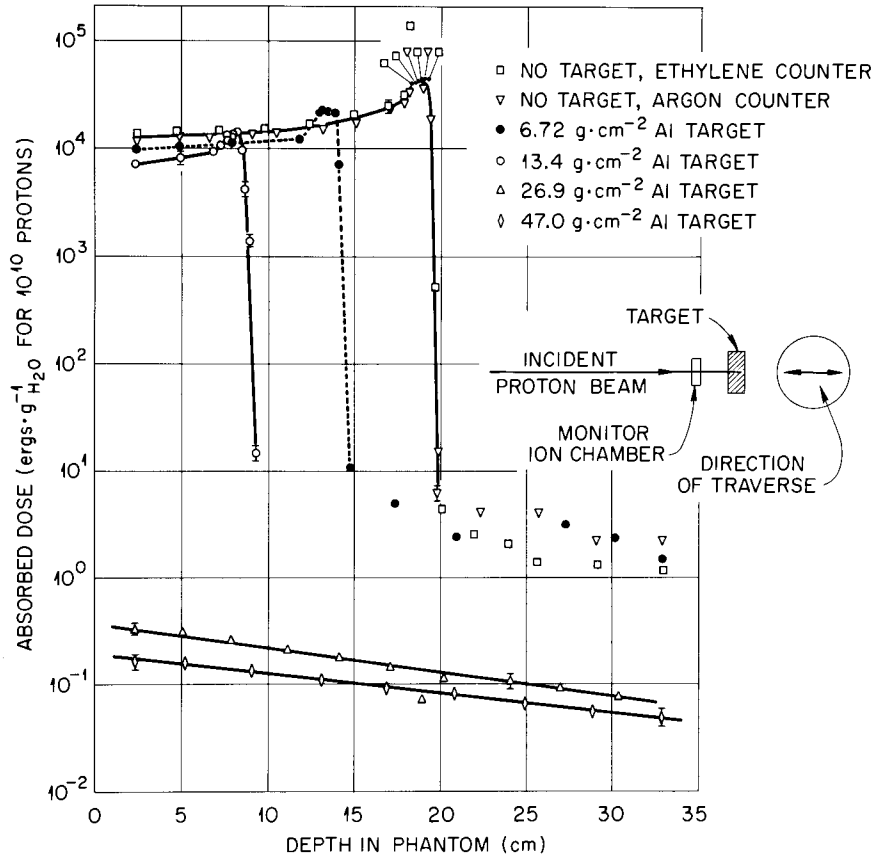


Fig. 8. Depth Dose Due to Nuclear Secondaries from 160-MeV Protons at 0°

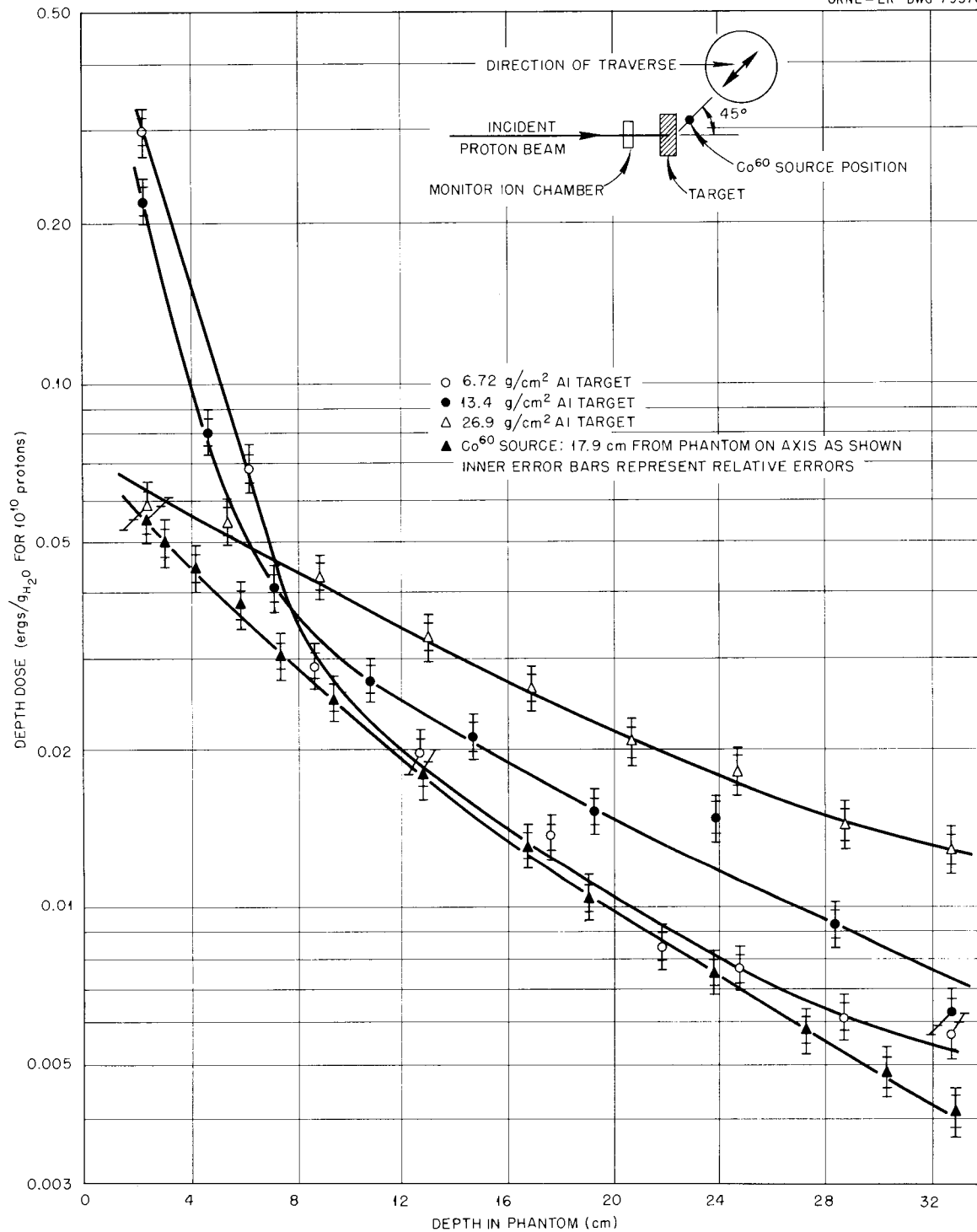


Fig. 9. Absorbed Dose as a Function of Depth in Phantom for Aluminum Targets of Three Thicknesses

the 160-MeV protons would be expected to be predominantly neutrons at the larger depths.

In Fig. 10 is shown the absorbed dose as a function of depth for four targets of widely varying Z . The dose increases with Z , as expected. The curve for the aluminum target appears to rise in relation to the curves for the other materials at large depths, but as shown, the errors for the aluminum target data are quite large, because of an abnormally high background during this measurement.

A limited number of traverses were made through the phantom in directions other than along the target-phantom axis. Three such traverses are shown in Fig. 11. The results appear reasonable when the geometries for secondary particle production are considered. In principle, by determining the depth dose along many such diameters, it is possible to ascertain the absorbed dose at all points throughout the phantom. The requirements for cyclotron operating time would be sizeable.

The smoothness of the data, especially that of Fig. 11, suggests that the relative errors shown may represent an overestimate.

No comparisons with theoretically predicted results are presented here. Even with the spherical geometry of the experiment, an elaborate transport calculation combined with appropriate secondary particle production cross sections is required. As previously stated, it is the purpose of these measurements to provide a standard against which such calculations may be tested.

Similar measurements are planned with incident proton beams of ~ 70 MeV.

V. ACKNOWLEDGMENTS

The series of nuclear secondary measurements at the Harvard University Synchrocyclotron, of which the present work is but one small part, was made possible only by the extraordinary cooperation extended by W. M. Preston and A. M. Koehler of the University. The beam-strength determinations were made by R. T. Santoro. M. M. Chiles designed and constructed the ion chamber, and T. F. Sliski and H. J. Stripling designed the ion-chamber drive and the phantom assembly.

UNCLASSIFIED
ORNL-LR-DWG 77653

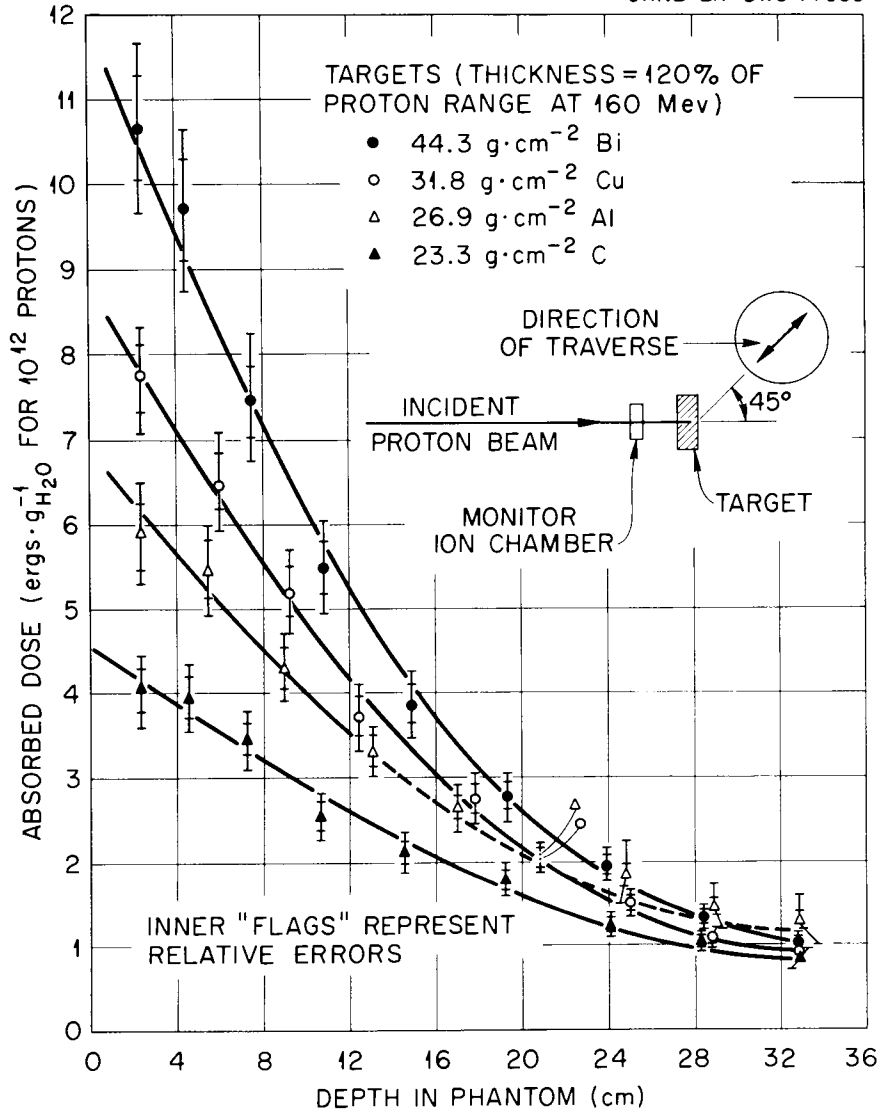


Fig. 10. Absorbed Dose as a Function of Depth in Phantom for Four Targets of Widely Varying Z

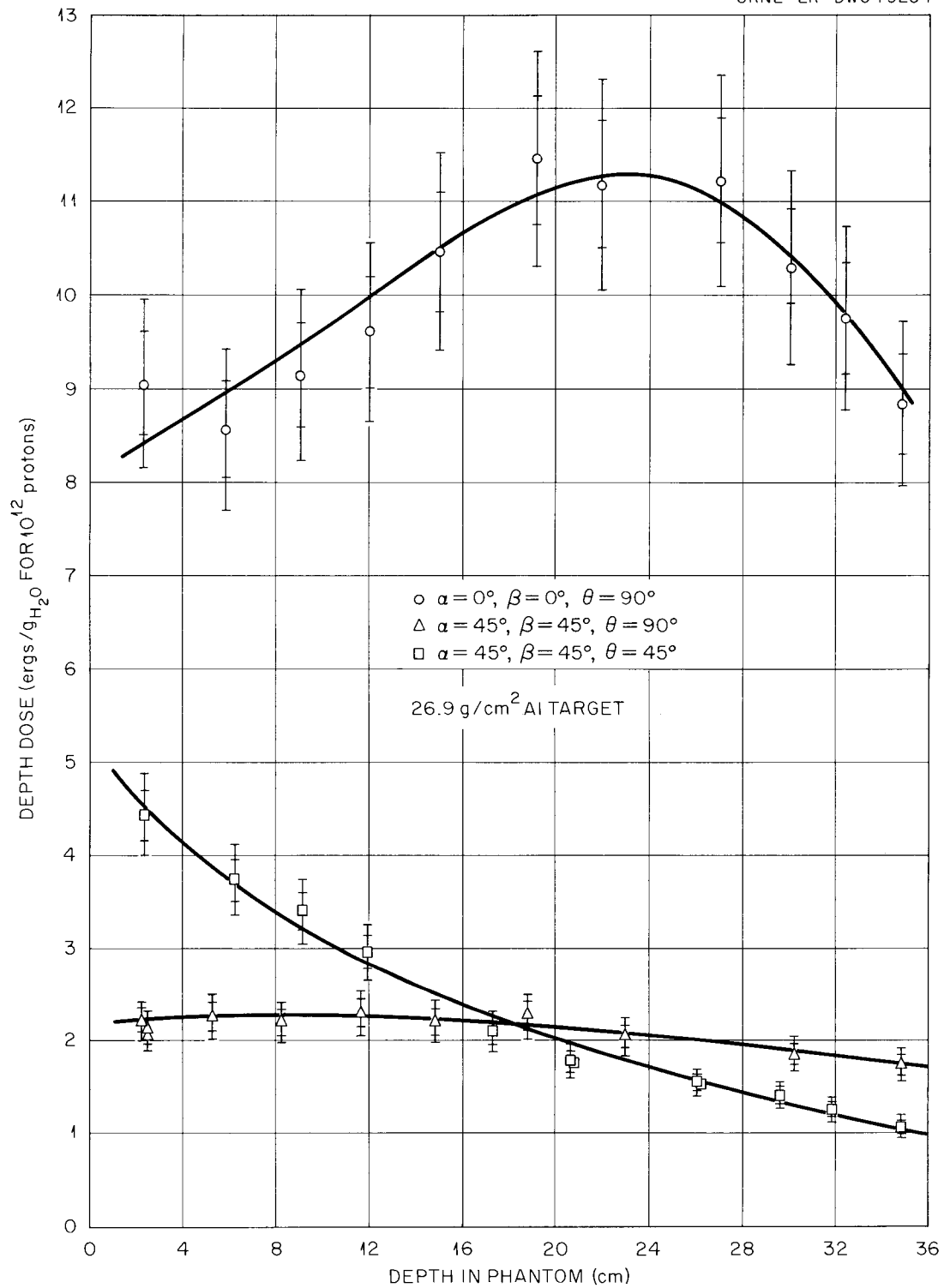


Fig. 11. Depth Dose Traverses at 45 and 90 deg from the Target-Phantom Axis

APPENDIX I

The values of the first collision dose tabulated and plotted on the following pages were computed according to the formula given in ref. 8.

Table I.1. First Collision Dose Versus Photon Energy for Specified Media.
(See also Figure I.1.)

Photon Energy (Mev)	Dose (erg /g for 10^7 photons/cm ²)				
	Lucite	Argon + 3% CO ₂	Ethylene	H ₂ O	Tissue
0.01	0.468	9.622	0.266	0.782	0.702
0.02	0.100	2.587	0.057	0.167	0.150
0.03	0.0424	1.148	0.025	0.070	0.063
0.04		0.605			
0.05	0.0214	0.376	0.018	0.031	0.029
0.06		0.229			
0.07	0.0235		0.025	0.032	0.031
0.08		0.155			
0.1	0.034	0.1135	0.038	0.040	0.038
0.2	0.086	0.0964	0.098	0.096	0.094
0.3	0.138	0.133	0.158	0.154	0.151
0.4		0.176			
0.5	0.238	0.217	0.272	0.264	0.260
0.6		0.259			
0.7	0.327		0.374	0.365	0.357
0.8		0.335			
1.0	0.447	0.406	0.511	0.498	0.488
2.0	0.750	0.687	0.856	0.832	0.816
3.0	0.980	0.931	1.110	1.09	1.07
4.0		1.167			
5.0	1.36	1.408	1.53	1.52	1.49
6.0		1.6787			
7.0	1.72	2.190	1.90	1.93	1.89
10.0	2.20	2.756	2.39	2.49	2.43

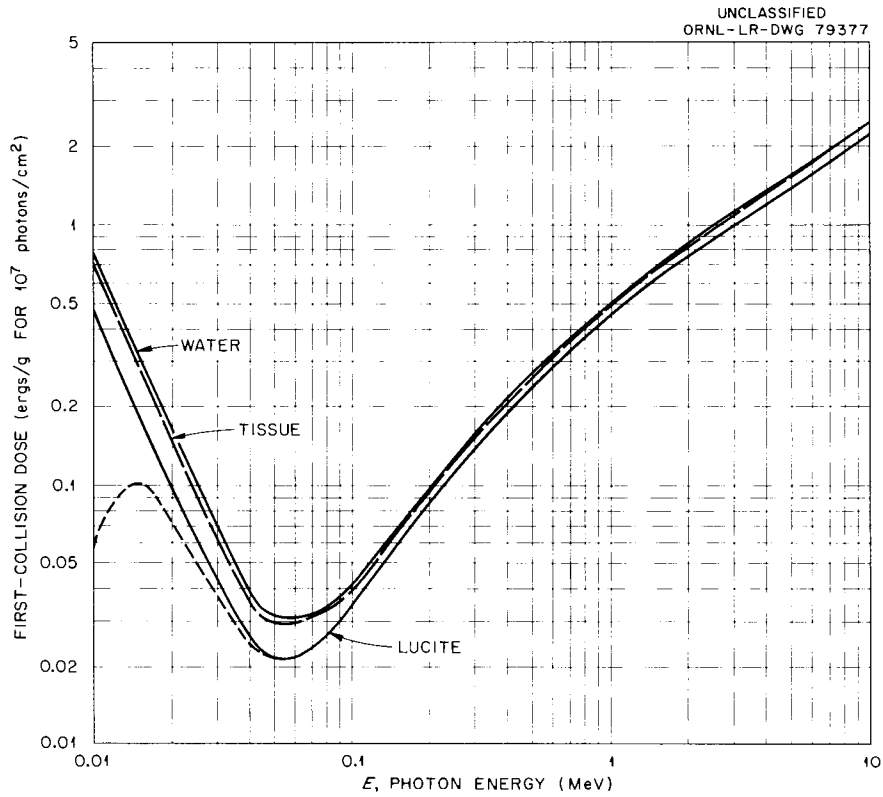


Fig. I.1. First-Collision Dose as a Function of Photon Energy for Water, Tissue, and Lucite. The broken-line portion of the lucite curve shows the probable low-energy response of the dosimeter to gamma rays.

APPENDIX II

TABLES OF EXPERIMENTAL RESULTS

Table II.1. Physical Dose Within a 42-cm-dia Water Phantom
as a Function of Ion Chamber Position. No target;
 10^{10} incident protons; $\alpha = \beta = 0^\circ$

Ethylene-Filled Chamber, $\theta = 0^\circ$		Argon-Filled Chamber, $\theta = 0^\circ$		Argon-Filled Chamber, $\theta = 90^\circ$	
Depth (cm)	Absorbed Energy (ergs/g of H ₂ O)	Depth (cm)	Absorbed Energy (ergs/g of H ₂ O)	Depth (cm)	Absorbed Energy (ergs/g of H ₂ O)
2.35	1.39 (4)*	2.35	1.27 (4)	2.35	1.97 (-1)
4.65	1.44 (4)	4.75	1.34 (4)	5.05	2.81 (-1)
7.15	1.49 (4)	6.55	1.38 (4)	8.45	4.39 (-1)
9.73	1.58 (4)	9.05	1.45 (4)	9.85	5.01 (-1)
		10.45	1.50 (4)	11.05	8.14 (-1)
12.35	1.71 (4)	12.65	1.61 (4)	11.85	1.17 (0)
				12.75	1.28 (0)
				12.85	1.22 (0)
				13.45	9.08 (-1)
				13.95	9.02 (-1)
14.95	2.04 (4)	15.05	1.87 (4)	15.05	1.07 (0)
				15.85	1.17 (0)
16.95	2.54 (4)	17.05	2.38 (4)	16.65	1.40 (0)
17.85	3.23 (4)	17.85	2.82 (4)	17.90	1.69 (0)
18.15	3.49 (4)	18.25	3.53 (4)		
18.35	4.02 (4)	18.55	4.11 (4)		
18.65	4.57 (4)	18.75	4.24 (4)	18.75	1.95 (0)
		18.85	4.20 (4)		
		18.93	4.16 (4)		
18.95	4.44 (4)	18.95	3.88 (4)		
19.25	4.66 (4)	19.15	3.41 (4)		
		19.35	1.94 (4)		
		19.55	5.60 (3)	19.85	2.03 (0)
19.65	5.25 (2)	19.75	6.26 (2)	20.75	2.11 (0)
20.05	4.48 (0)	19.95	1.57 (1)	21.65	2.12 (0)
21.95	2.58 (0)	22.35	4.15 (0)	22.75	1.96 (0)
				23.95	1.72 (0)
				24.65	1.55 (0)
25.65	1.42 (0)	25.65	4.05 (0)	26.35	1.06 (0)
29.15	1.38 (0)	29.05	2.26 (0)	28.65	7.16 (-1)
32.85	1.23 (0)	32.85	2.30 (0)	32.85	4.43 (-1)

*Digit in parentheses indicates power-of-ten multiplier, i.e., 1.39 (4) \equiv 1.39 x 10⁴.

Table II.2. Physical Dose Rate Within a 42-cm-dia Water Phantom as a Function of Ion Chamber Position, for a Co^{60} Gamma-Ray Source.*
 Source-Phantom Distance: 17.9 cm.
 $\alpha = \beta = \theta = 0^\circ$.

Argon-Filled Ion Chamber		Ethylene-Filled Ion Chamber	
Depth (cm)	Absorbed Energy ($\text{ergs} \cdot \text{g}_{\text{H}_2\text{O}}^{-1} \cdot \text{sec}^{-1}$)	Depth (cm)	Absorbed Energy ($\text{ergs} \cdot \text{g}_{\text{H}_2\text{O}}^{-1} \cdot \text{sec}^{-1}$)
2.35	5.48 (-2)	2.45	5.31 (-2)
3.05	4.95 (-2)	2.95	5.04 (-2)
4.25	4.44 (-2)	4.15	4.31 (-2)
5.85	3.79 (-2)	5.85	3.58 (-2)
7.45	3.03 (-2)		
7.45**	3.06 (-2)	8.05	2.64 (-2)
		8.05**	2.79 (-2)
9.45	2.51 (-2)		
		11.35	1.91 (-2)
		11.35**	2.03 (-2)
12.85	1.85 (-2)		
		14.85	1.41 (-2)
16.85	1.32 (-2)		
		17.85	1.05 (-2)
19.55	1.04 (-2)		
19.55**	1.05 (-2)	20.95	0.84 (-2)
23.85	0.76 (-2)		
27.35	0.59 (-2)		
30.35	0.48 (-2)		
32.95	0.41 (-2)		

*Source strength: 2.38×10^{-4} r/sec at 1 m, National Bureau of Standards calibration.

**Repeated measurement.

Table II.3. Physical Dose Within a 42-cm-dia Water Phantom as a Function of Ion Chamber Position. Target: H_2O , 21.1 g/cm^2 ; argon-filled chamber; $\alpha = \beta = \theta = 0^\circ$; 10^{10} incident photons; target-phantom distance: 48.5 cm.

Depth (cm)	Absorbed Energy (ergs/g of H_2O)
2.35	1.27 (-1)
4.85	1.12 (-1)
7.35	9.65 (-2)
9.75	8.48 (-2)
12.95	7.44 (-2)
16.25	6.68 (-2)
19.85	5.68 (-2)
22.95	5.26 (-2)
26.15	4.43 (-2)
29.45	3.68 (-2)
32.85	3.25 (-2)

Table II.4. Physical Dose Within a 42-cm-dia Water-Filled Phantom as a Function of Ion Chamber Position for Various Thicknesses of Aluminum Target.
 Target-phantom distance: 48.5 cm; $\alpha = \beta = \theta = 0^\circ$;
 10^{10} incident photons.

Argon-Filled Ion Chamber				Ethylene-Filled Ion Chamber*			
Target Thickness: 6.72 g/cm ²		Target Thickness: 13.4 g/cm ²		Target Thickness: 26.9 g/cm ²		Target Thickness: 47.0 g/cm ²	
Depth (cm)	Absorbed Energy (ergs/g of H ₂ O)	Depth (cm)	Absorbed Energy (ergs/g of H ₂ O)	Depth (cm)	Absorbed Energy (ergs/g of H ₂ O)	Depth (cm)	Absorbed Energy (ergs/g of H ₂ O)
2.35	9.97 (3)	2.35	7.29 (3)	2.35	3.31 (-1)	2.35	1.74 (-1)
4.95	1.03 (4)	4.95	8.17 (3)	5.05	3.12 (-1)	5.25	1.70 (-1)
		6.85	9.24 (3)				
		7.25	1.05 (4)				
		7.65	1.38 (4)				
7.85	1.09 (4)	7.65**	1.25 (4)	7.85	2.68 (-1)		
		7.85	1.29 (4)				
		7.95	1.31 (4)				
		8.25	1.46 (4)			9.05	1.42 (-1)
		8.45	9.64 (3)				
		8.65	4.14 (3)				
		8.95	1.36 (3)				
		9.25	1.50 (1)				
10.85	1.30 (4)	10.84	1.91 (1)	11.15	2.18 (-1)		
11.75	1.48						
12.95	2.21						
13.15	2.32					13.15	1.18 (-1)
13.45	2.29						
13.85	1.52						
14.05	7.12 (3)			14.15	1.81 (-1)		
14.75	1.08 (1)	14.75	1.47 (1)				
17.35	4.96 (0)			17.15	1.50 (-1)	16.85	9.75 (-2)
		18.05	1.33 (1)				
				18.85	0.70 (-1)		
20.95	2.46 (0)	21.05	1.09 (1)	20.25	1.22 (-1)	20.85	8.39 (-2)
23.95	2.13 (0)	23.85	1.10 (1)	24.05	1.09 (-1)	24.95	6.75 (-2)
27.35	3.16 (0)	27.35	1.18 (1)	26.95	0.93 (-1)		
30.05	2.63 (0)	30.05	9.56 (0)	30.45	0.79 (-1)	28.85	5.77 (-2)
32.85	1.43 (0)	32.85	8.91 (0)			32.85	4.94 (-2)

*A comparison of the response of the ethylene-filled chamber with that of the argon-filled chamber under identical conditions is shown in Table II.2.

**Repeated measurement.

Table II.5. Physical Dose Within a 42-cm-dia Water Phantom as a Function of Ion Chamber Position. 26.9 g/cm²-thick aluminum target; $\alpha = \beta = 0^\circ$; 10^{10} incident photons; target-phantom distance: 48.5 cm.

Argon-Filled Chamber $\theta = 0^\circ$		Argon-Filled Chamber $\theta = 90^\circ$	
Depth (cm)	Absorbed Energy (ergs/g of H ₂ O)	Depth (cm)	Absorbed Energy (ergs/g of H ₂ O)
2.35	2.45 (-1)	2.35	9.01 (-2)
4.15	2.41 (-1)		
5.35	2.31 (-1)	5.85	8.56 (-2)
6.55	2.18 (-1)		
8.45	1.87 (-1)	9.05	9.14 (-2)
11.35	1.64 (-1)	11.95	9.61 (-2)
14.45	1.42 (-1)	15.05	1.05 (-1)
17.65	1.21 (-1)	19.15	1.14 (-1)
20.55	9.92 (-2)	21.95	1.12 (-1)
23.35	8.73 (-2)	25.05	1.12 (-1)
27.05	7.74 (-2)	28.05	1.03 (-1)
29.85	7.03 (-2)	30.35	9.74 (-2)
32.85	6.10 (-2)	32.85	8.84 (-2)

Table II.6. Physical Dose Within a 42-cm-dia Water Phantom as a Function of Ion Chamber Position, for Two Target Thicknesses.
 Argon-Filled Ion Chamber, $\alpha = \beta = 45^\circ$; $\theta = 0^\circ$;
 target-phantom distance: 53.7 cm.

6.72 g/cm ² Al Target		13.4 g/cm ² Al Target	
Depth (cm)	Absorbed Energy (ergs/g of H ₂ O)	Depth (cm)	Absorbed Energy (ergs/g of H ₂ O)
2.35	2.98 (-1)	2.35	2.20 (-1)
6.25	6.88 (-2)	4.75	8.02 (-2)
8.75	2.90 (-2)	7.25	4.08 (-2)
12.75	1.99 (-2)	10.85	2.74 (-2)
16.75	1.38 (-2)	14.75	2.14 (-2)
21.85	0.85 (-2)	19.35	1.54 (-2)
24.85	0.77 (-2)	23.95	1.15 (-2)
28.85	0.62 (-2)	28.45	0.94 (-2)
32.85	0.57 (-2)	32.85	(0.63 (-2))

Table II.7. Physical Dose Within a 42-cm-dia Water Phantom as a Function of Ion Chamber Position for Traverses at Various Angles, θ , from the Target-Phantom Axis. Aluminum target, 26.9 g/cm^2 ; argon-filled ion chamber: $\alpha = \beta = 45^\circ$; target-phantom distance: 53.7 cm .

$\theta = 0^\circ$		$\theta = 45^\circ$		$\theta = 90^\circ$	
Depth (cm)	Absorbed Energy (ergs/g of H_2O)	Depth (cm)	Absorbed Energy (ergs/g of H_2O)	Depth (cm)	Absorbed Energy (ergs/g of H_2O)
2.35	5.91 (-2)	2.35	4.43 (-2)	2.25	2.21 (-2)
				2.35	2.13 (-2)
				2.35	2.07 (-2)
				5.25	2.27 (-2)
5.45	5.47 (-2)	6.25	3.73 (-2)		
8.95	4.28 (-2)	9.15	3.40 (-2)	8.20	2.20 (-2)
13.05	3.29 (-2)	11.95	2.95 (-2)	11.65	2.30 (-2)
16.95	2.64 (-2)	17.35	2.10 (-2)	14.85	2.21 (-2)
20.75	2.09 (-2)	20.65	1.78 (-2)	18.85	2.27 (-2)
		20.85	1.77 (-2)		
		24.05	1.56 (-2)	22.95	2.04 (-2)
24.75	1.84 (-2)	24.25	1.52 (-2)		
		27.65	1.39 (-2)		
28.85	1.45 (-2)	29.85	1.24 (-2)	28.25	1.85 (-2)
32.85	1.30 (-2)	32.85	1.06 (-2)	32.85	1.74 (-2)

Table II.8. Physical Dose Within a 42-cm-dia Water Phantom as a Function of Ion Chamber Position, for Targets of Carbon ($z = 6$), Copper ($z = 29$), and Bismuth ($z = 83$). Argon-filled ion chamber; $\alpha = \beta = 45^\circ$; $\theta = 0^\circ$; 10^{10} incident photons; target-phantom distance: 53.7 cm.

Carbon Target (23.3 g/cm ²)		Copper Target (20 cm dia, 31.8 g/cm ²)		Copper Target (40 cm dia, 31.8 g/cm ²)		Bismuth Target (44.3 g/cm ²)	
Depth (cm)	Absorbed Energy (ergs/g of H ₂ O)	Depth (cm)	Absorbed Energy (ergs/g of H ₂ O)	Depth (cm)	Absorbed Energy (ergs/g of H ₂ O)	Depth (cm)	Absorbed Energy (ergs/g of H ₂ O)
2.35	4.06 (-2)	2.35	7.76 (-2)	2.35	6.22 (-2)	2.35	1.07 (-1)
4.55	3.94 (-2)					4.45	9.71 (-2)
		5.95	6.47 (-2)	6.15	6.49 (-2)		
7.25	3.45 (-2)					7.45	7.45 (-2)
		9.25	5.18 (-2)	9.05	4.37 (-2)		
10.65	2.53 (-2)					10.85	5.50 (-2)
		12.35	3.72 (-2)	12.25	3.32 (-2)		
14.55	2.11 (-2)					14.85	3.87 (-2)
		16.65	2.73 (-2)	16.85	2.28 (-2)		
19.15	1.77 (-2)					19.25	2.77 (-2)
		20.85	2.06 (-2)	20.65	1.91 (-2)		
				23.85	1.52 (-2)		
24.05	1.24 (-2)	24.95	1.51 (-2)			23.85	1.95 (-2)
				26.85	1.15 (-2)		
28.25	1.03 (-2)	28.75	1.11 (-2)			28.45	1.34 (-2)
				29.85	1.07 (-2)		
32.85	0.84 (-2)	32.85	0.94 (-2)	32.85	0.88 (-2)	32.85	1.02 (-2)



ORNL-3457
 UC-34 - Physics
 TID-4500 (20th ed.)

INTERNAL DISTRIBUTION

- | | |
|-------------------------------------|---------------------------------|
| 1. Biology Library | 51. W. E. Kinney |
| 2-3. Central Research Library | 52. C. E. Larson |
| 4. Reactor Division Library | 53-77. F. C. Maienschein |
| 5-6. ORNL - Y-12 Technical Library | 78. J. W. Paul |
| Document Reference Section | 79. F. W. Sanders |
| 7-41. Laboratory Records Department | 80. M. J. Skinner |
| 42. Laboratory Records, ORNL R.C. | 81. J. A. Swartout |
| 43. R. G. Alsmiller, Jr. | 82. J. E. Turner |
| 44. J. A. Auxier | 83. A. M. Weinberg |
| 45. E. P. Blizard | 84. C. D. Zerby |
| 46. T. V. Blosser | 85. W. Zobel |
| 47. Marion M. Chiles | 86. R. A. Charpie (consultant) |
| 48. W. A. Gibson | 87. P. F. Gast (consultant) |
| 49. F. F. Haywood | 88. R. F. Taschek (consultant) |
| 50. W. H. Jordan | 89. T. J. Thompson (consultant) |

EXTERNAL DISTRIBUTION

90. Research and Development Division, AEC, ORO
 91-727. Given distribution as shown in TID-4500 (20th ed.) under Physics category (75 copies - OTS)